IEEE Access
Multidisciplinary | Rapid Review | Open Access Journal

Received December 27, 2019, accepted January 8, 2020, date of publication January 13, 2020, date of current version January 24, 2020.

Digital Object Identifier 10.1109/ACCESS.2020.2966257

Tri-Band Band-Pass Filter Based on Multi-Mode Spoof Surface Plasmon Polaritons

HONGXIN ZHAO[1], (Member, IEEE), PENG ZHOU[1], (Student Member, IEEE), ZHIXIA XU[1], (Student Member, IEEE), SHUNLI LI[1], (Member, IEEE), MEI YANG[2], (Member, IEEE), LEILEI LIU[2], (Member, IEEE), AND XIAOXING YIN[1], (Member, IEEE)

[1]State Key Laboratory of Millimeter Waves, School of Information Science and Engineering, Southeast University, Nanjing 210096, China
[2]National and Local Joint Engineering Laboratory of RF Integration and Micro-Assembly Technology, Nanjing University of Posts and Telecommunications, Nanjing 210003, China

Corresponding author: Hongxin Zhao (zhaohongxin@seu.edu.cn)

This work was supported in part by the National Natural Science Foundation of China under Grant 61771127, Grant 61801116, Grant 61701257, and Grant 61427801, and in part by the open research fund of the National and Local Joint Engineering Laboratory of RF Integration and Micro-Assembly Technology under Grant KFJJ20180101.

ABSTRACT This paper presents a novel tri-band bandpass filter based on multi-mode spoof surface plasmon polaritons (SSPPs) in microwave frequencies. The combination of multi-mode resonance and cutoff characteristic of SSPPs contributes to a tri-band bandpass response. The proposed SSPPs-based filter consists of two coplanar waveguides, two conversion parts and a SSPPs transmission structure made of five unit-cells. Each unit cell is a multi-mode resonator, which is constructed by a pair of oppositely oriented double-side folded strips, and the ends of folded strips are placed closely to form coupled-stubs. Two distinct passbands divided by a sharp stopband are produced under the cutoff frequency of SSPPs transmission structure. The third passband above the cutoff frequency is introduced by the resonant tunneling effect due to the self-resonant mode of proposed SSPPs unit cell. Dispersion relations, electric field distributions and proposed equivalent transmission line model give a physical insight into the filter operating mechanism. As a demonstration, a prototype of the proposed filter has been fabricated and measured. The measurement results demonstrate that the proposed filter has a tri-band bandpass performance with excellent frequency selectivity, which may be very useful in many applications, such as multi-band wireless systems.

INDEX TERMS Multi-mode resonator, resonant tunneling effect, spoof surface plasmon polaritons (SSPPs), tri-band bandpass filter.

I. INTRODUCTION

Due to the negative permittivity characteristic of metals in optical frequencies, surface plasmon polaritons (SPPs) as special surface waves propagate parallel to the interface of dielectrics and metals, but attenuate exponentially in the transverse direction [1], [2]. Thus, SPPs exhibit superior abilities of field confinement along the interface and local-field enhancement in sub-wavelength scale [3], [4], which ensure SPPs have promising applications in optical circuits and near-field microscopy [5], [6]. However, the natural SPPs cannot exit in microwave frequencies since metals behave as perfect conductors in these frequency bands. To extend the applications of SPPs in the lower frequencies, the so-called spoof SPPs (SSPPs) structures with arrays of grooves and holes are proposed to support surface bound modes [7], [8]. Subsequently, the applications of SSPPs in microwave and terahertz frequencies have attracted much interest of researchers, such as novel high-efficiency SSPPs transmission structures [9]–[11], filters [12]–[14], splitters [15], [16] and antennas [17]–[20].

The intrinsic slow-wave characteristic of SSPPs is advantageous in the designs of various microwave filters with different features such as ultra-wideband, band-stop or multi-band performances. In the previous works, the SSPPs-based ultra-wideband band-pass filters are usually realized by the hybrid structures of substrate integrated waveguides (SIWs), half-mode SIWs (HMSIWs) and different SSPPs [21]–[23], or introducing gap coupling between multi-stage SSPPs transmission lines and resonators [24]–[27]. Researches have

The associate editor coordinating the review of this manuscript and approving it for publication was Nosherwan Shoaib.

demonstrated that the upper passband cutoff frequencies of these filters can be independently adjusted by the geometrical parameters of SSPPs waveguides. In addition, in order to realize band-rejection responses for practical applications, series of band-stop filters are proposed by etching split-ring resonators (SRRs) [28] or complementary SRRs (CSRRs) [29] in the traditional SSPPs structures with corrugated strips. It differs from the bandpass filters based on the magnetic coupling between planar Goubau line and resonators [30], [31], since the resonant modes of SRRs or CSRRs are excited effectively by the electric field components of SSPPs modes perpendicular to the strip surface, leading to a stopband near the resonant frequencies. Band-stop filters operating in the similar mechanism are also achieved by loading resonators near the corrugated strips [32], [33]. It is found that the rejection performances of the band-stop filters mentioned above are all realized by loading extra resonators. This method will increase the complexity of filter design. Furthermore, the band pass or band stop performances currently reported are all realized under SSPPs cutoff frequencies. Recently, the tunneling above SSPPs cutoff frequencies is realized by loading small SRRs to support magnetoinductive waves propagation [34]. However, the insertion loss of the reported tunneling is a little bit large since the interactions between SRRs and SSPPs exist in the lossy medium. The inevitable ripple within the tunneling band also degrades its performances. Moreover, several approaches are proposed to design SSPPs-based filters with multi-band performances. In [35], two novel dual-band bandpass filters are proposed based on multilayers, which have effective permittivities of opposite signs in certain frequency ranges to support SPPs-like propagation. These two filters show excellent in-band characteristics and selectivity confirmed by measurement results, but its bandwidth of passbands is relatively small. In addition, multi-mode resonator, as a widely employed concept in microwave filters [36], is also utilized to design wideband and multi-band SSPPs filters with compact sizes. Several filters based on SSPPs high-order modes [37] or localized SPPs [38] have demonstrated its potential applications in multi-band uses owing to multi-mode characteristics. However, tri-band filters based on multi-mode SSPPs are rarely reported.

To meet the increasing demand of multi-band filters in modern wireless systems, this paper presents a novel SSPPs-based filter to achieve tri-band bandpass performances. Each SSPPs unit cell in this filter behaves as a multi-mode resonator, which is constructed by a pair of oppositely oriented double-side folded strips. The ends of folded metallic strips are placed closely to form the coupled-stubs. Compared with the previous works, the highlights of the proposed SSPPs-based filter are summarized as follow. Firstly, compared with interdigital capacitance loaded loop resonators in [39], this work presents a simpler but efficient multi-mode SSPPs unit-cell, and achieves tri-band bandpass performances. Secondly, the multiple resonant modes of the SSPPs unit cell show more flexible tunability, and can be used to produce stopband and passband simultaneously, which is advantageous for the multi-band filters design. In this work, the first stopband under the SSPPs cutoff frequency is generated by the resonance of coupled-stubs in each SSPPs unit cell, instead of loading any extra resonators. Compared with [39], the rejection bands between adjacent passbands are wider. Dispersion relations have demonstrated that the first stopband can be flexibly controlled by the physical dimensions of SSPPs unit cell. The self-resonance of SSPPs unit cell realizes the resonant tunneling effect above the SSPPs cutoff frequency and produces the third passband, demonstrating another approach to realize the passband performances above the SSPPs cutoff frequency. Compared with the tunneling supported by magnetoinductive waves propagation [34], the resonant tunneling effect in our work shows evident advantages including lower insertion loss and excellent frequency selectivity with fairly small ripples.

II. PROPOSED SSPPS-BASED FILTER AND ANALYSIS

A. SIMULATION RESULTS AND DISCUSSION

Fig. 1(a) depicts the top view of the proposed SSPPs-based filter, which is constructed by five concatenated sections with three construction elements named as part I, II, and III. As can be observed, the feeding structures of the proposed filter are two coplanar waveguides (CPWs) in part I. The dimensions of CPWs are designed properly to achieve 50Ω impedance match with standard SMA connectors for practical applications. In order to realize highly efficient conversion from quasi-TEM mode of CPW to SSPPs TM mode, gradient metallic strips and flaring grounds with exponential outlines are employed in part II to realize impedance and momentum match, as shown in Fig. 1(b). The exponential contour line of the upper flaring ground is determined by the starting point $P_1(x_1, y_1)$ and ending point $P_2(x_2, y_2)$, and is expressed as:

$$y = C_1 e^{\alpha x} + C_2 \tag{1}$$

where $C_1 = \frac{y_2 - y_1}{e^{\alpha x_2} - e^{\alpha x_1}}$, and $C_2 = \frac{y_1 e^{\alpha x_2} - y_2 e^{\alpha x_1}}{e^{\alpha x_2} - e^{\alpha x_1}}$.

The optimized α is chosen as 0.16 in this design. Part III shown in Fig. 1(c) is the double-side corrugated SSPPs transmission structure consisting of five unit-cells. Different from the previous works, the proposed SSPPs unit cell is composed of two oppositely oriented double-side folded strips, in which the ends of metallic strips are placed closely to form coupled-stubs. In this scenario, multiple resonant modes are excited in the SSPPs unit cell.

The simulated transmission and reflection coefficients of the proposed filter are depicted in Fig. 1(d). It can be seen that a narrow but deep stopband is realized from 3.8 GHz to 4.6 GHz with −10dB rejection level ($S_{21} < -10$dB), contributing to the good frequency isolation of the first and second passbands. For the first passband, the reflection coefficient S_{11} can be kept lower than −10 dB from 1.4 to 3.6 GHz, and the poor reflection performances below 1.4 GHz are determined by the cutoff frequency characteristic of single conductor similar to Goubau line [40]. The good impedance match performance is also achieved from 5 to 7 GHz within the second passband (S_{11} <-10dB). The higher

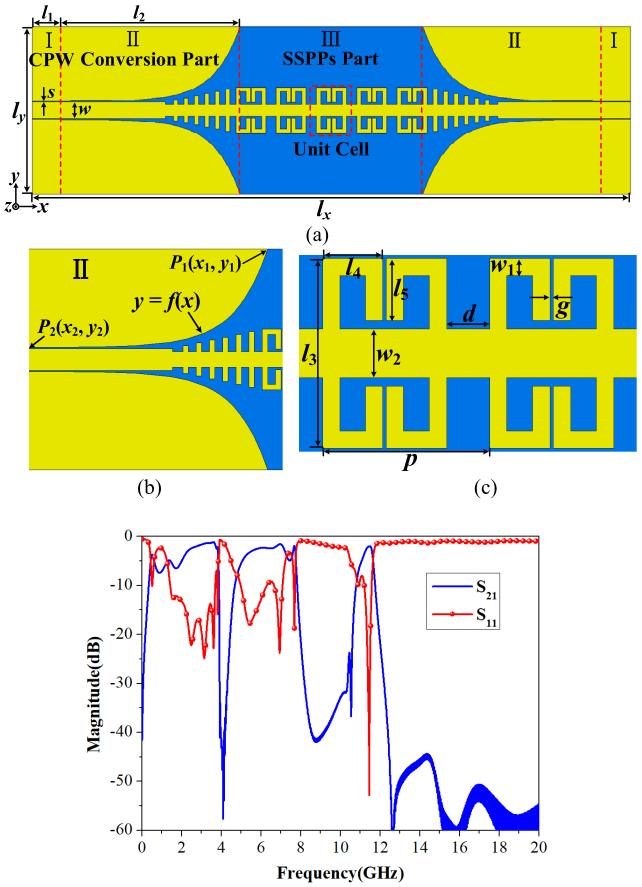

FIGURE 1. (a) Top view of the proposed SSPPs-based filter. Detailed dimensions are determined as: $l_x = 144$mm, $l_y = 40$mm, $l_1 = 5$mm, $l_2 = 45$mm, $s = 0.2$mm, $w = 3.94$mm. (b) Conversion part. (c) The proposed SSPPs unit cells. Detailed dimensions are determined as: $l_3 = 11$mm, $l_4 = 3.5$mm, $l_5 = 3.6$mm, $w_1 = 1$mm, $w_2 = 2.8$mm, $d = 2.5$mm, $g = 0.2$mm, $p = 9.7$mm. (d) Simulated S-parameters of the proposed filter. The proposed filter is designed on a Rogers 4350B dielectric substrate with thickness of 0.508mm, it's dielectric constant ε_r is set as 3.48 and it's loss tangent is set as 0.0037 for simulations. The conductor material is chosen as tin, and it's thickness is set as 0.035mm. The structure is analyzed by CST microwave studio.

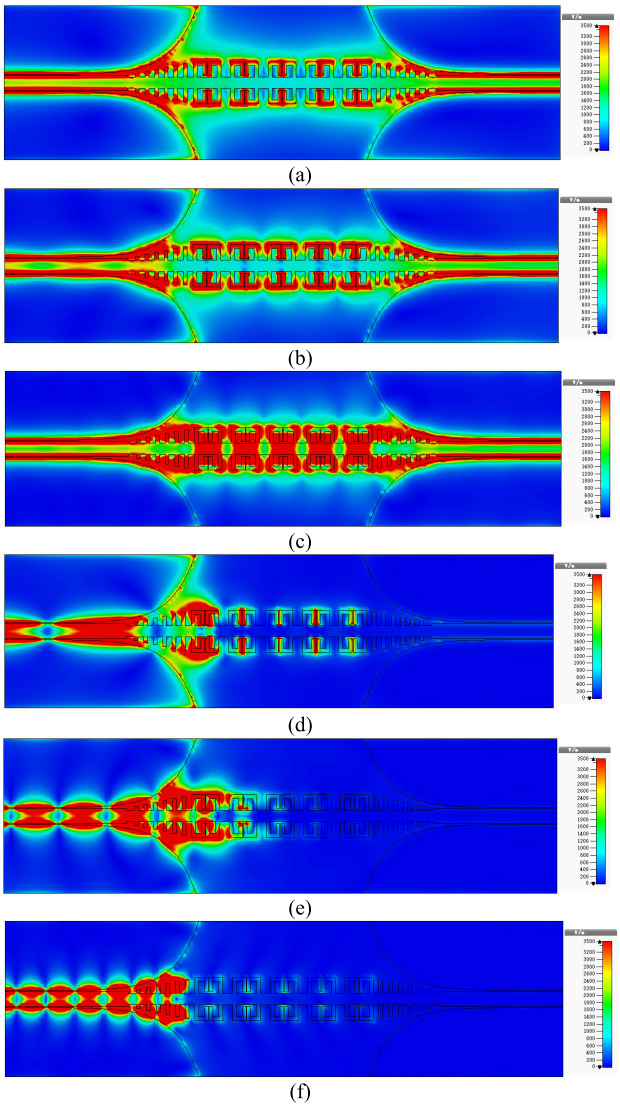

FIGURE 2. Simulated electric field distributions of the proposed SSPPs-based filter at different frequencies. (a) 2.5GHz within the first passband. (b) 6GHz within the second passband. (c) 11.4GHz within the third passband. (d) 4GHz within the first stopband. (e) 9GHz within the second stopband. (f) 15GHz within the highest stopband.

cutoff frequency of second passband is determined by the proposed SSPPs structure. Furthermore, as an attractive phenomenon, a narrow passband appears above the SSPPs cutoff frequency with a transmission pole located at 11.4 GHz. The simulation results demonstrate that the characteristic of the third passband is fairly good with excellent frequency selectivity and low insertion loss of 1.9 dB at its center frequency.

In order to give a physical insight into the operating mechanism of the proposed filter, the simulated electric field distributions on $x - o - y$ plane are displayed in Fig. 2. Fig. 2(a) to (c) are the simulated field distributions at different frequencies within three passbands, respectively. It is obvious that the electric field energy at these three frequencies can propagate from the left port to the right port with low transmission loss, which demonstrates the excellent transmission performances of three passbands. Meanwhile, as shown in Fig. 2(a) and (b), the similar electric field distributions indicate that both of the first and second passbands are supported by SSPPs mode. However, different from the first and second passbands, it is observed in Fig. 2(c) that the third passband is generated by the self-resonance of proposed SSPPs unit cell, and supported by the resonant tunneling effect. In addition, the simulated field distributions at different frequencies within three stopbands are shown in Fig. 2(d) to (f), respectively. As illustrated in Fig. 2(d), the electric field energy is mainly concentrated on the localized regions of coupled-stubs, and cannot propagate through SSPPs structure, indicating that the first stopband is generated by the resonance of coupled-stubs. Moreover, the second and third stopbands are determined by the cutoff frequencies of proposed SSPPs unit cell and conversion part respectively, since the electric field energy is blocked near the first SSPPs unit cell and conversion part, as depicted in Fig. 2(e) and (f).

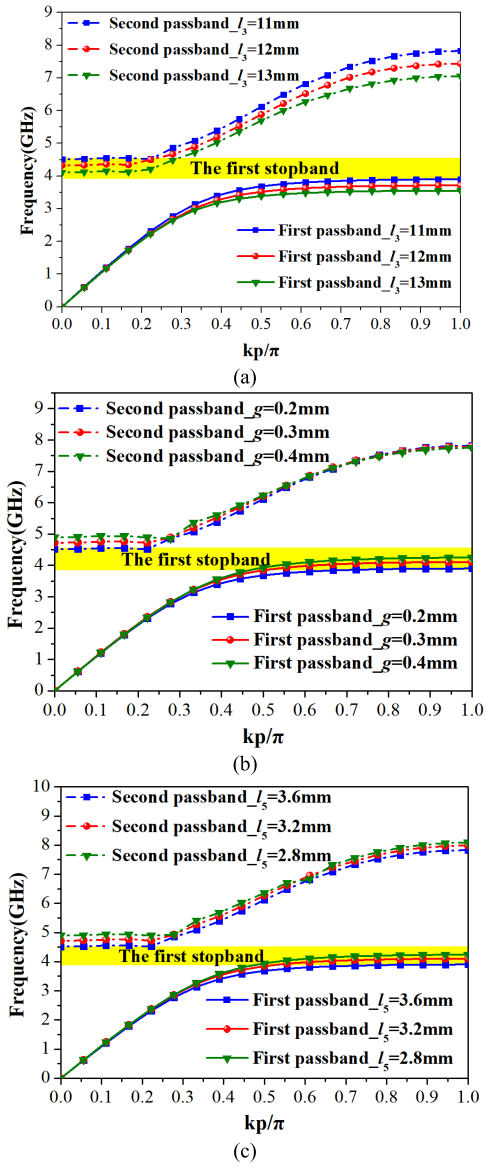

FIGURE 3. Dispersion relations of SSPPs modes with respect to key geometrical parameters. (a) Variation of dispersion relations with different l_3. (b) Variation of dispersion relations with different g. (c) Variation of dispersion relations with different l_5.

On the basis of above analysis, we can draw a conclusion that the proposed SSPPs structure operates in three different modes. The first mode is SSPPs mode supporting the first and second passbands propagation. The second mode is generated by the resonance of coupled-stubs in SSPPs unit cell, which can produce a narrow stopband and lead to the split of SSPPs mode into two passbands. The third mode is the self-resonance of SSPPs unit cell and supports the resonant tunneling effect above the SSPPs cutoff frequencies.

Fig. 3 shows the variations of SSPPs dispersion relations with respect to the key geometrical parameters. As illustrated in Fig. 3(a), keeping other parameters unchanged, the dispersion curves of two passbands supported by SSPPs mode gradually shift to the lower frequencies with the increase of the height l_3 of the unit cell. The frequency gap between the first and second passbands is the first stopband, which decreases to the lower frequencies with almost unchanged bandwidth when l_3 is varied from 11 to 13mm. The upper cut-off frequencies of the second passbands have demonstrated the good field confinement ability of the proposed SSPPs unit cell. In addition, it is obvious that the parameters of coupled-stubs have significant influence on the SSPPs dispersion relations, as shown in Fig. 3(b) and (c), respectively. As the coupling gap of coupled-stubs g increases, the upper cutoff frequencies of the second passband are not affected while the first stopband gradually shifts to the higher frequencies. Furthermore, with the decrease of the length l_5 of coupled-stubs, the upper cutoff frequencies of the second passband as well as the first stopband will shift to the higher frequencies. The variations of the first stopband shown in Fig. 3(b) and (c) can be attributed to the weakened coupling of coupled-stubs with the increase of g or the decrease of l_5. Generally, the first stopband can be flexibly controlled by properly designing the parameters of coupled-stubs.

Fig. 4 investigates the influence of key parameters on the filter performances while keeping other parameters unchanged. As shown in Fig. 4(a), with the increase of l_3, the first transmission zero f_{z1} shifts to the lower frequencies while the third passband shifts to the higher frequencies. Conversely, Fig. 4(b) shows that increasing g contributes to the increase of f_{z1} and the decrease of the third passband. In addition, f_{z1} as well as the third passband simultaneously shifts to the higher frequencies with the decrease of l_5, as shown in Fig. 4(c). It is clear that the variation tendency of f_{z1} with respect to different parameters shows good consistency with the first stopband shown in Fig. (3), since the first stopband is generated by f_{z1}. The parametric study shown in Fig. 4 have demonstrated that $f_{z1}$is more sensitive to the small variations of g.

The current vector distribution of SSPP unit cell within the third passband is displayed in Fig. 5. It is evident that the resonance of entire SSPPs unit cell can be regarded as the combination of four SRR resonant modes. Therefore, the variations of the third passband shown in Fig. 4 can be attributed to different reasons. As shown in Fig. 4(a), as l_3 increases, the coupling capacitor C_1 within each SRR will decrease significantly, and thus lead to the increase of the third passband and larger insertion loss. Similarly, the decline of l_5 will decrease C_1 and the resonant length of SRR, leading to larger insertion loss, and the increase of the third passband shown in Fig. 4(c). Generally, the decrease of C_1 will lead to the decline of efficiency of SRR resonant mode, and contribute to the larger insertion loss of the third passband.

To reduce the insertion loss of the third passband, the relative length $(l_3 - l_5 \times 2 - w_2)/2$ should be kept as small as possible in practical design to ensure the efficiency of SRR resonant mode. Considering the precision of fabrication process, the relative length is finally determined as 0.2mm. Furthermore, with the increase of g, the third passband gradually shifting to the lower frequencies is due to the increase of total resonant length of SSPP unit cell, as shown in Fig. 4(b).

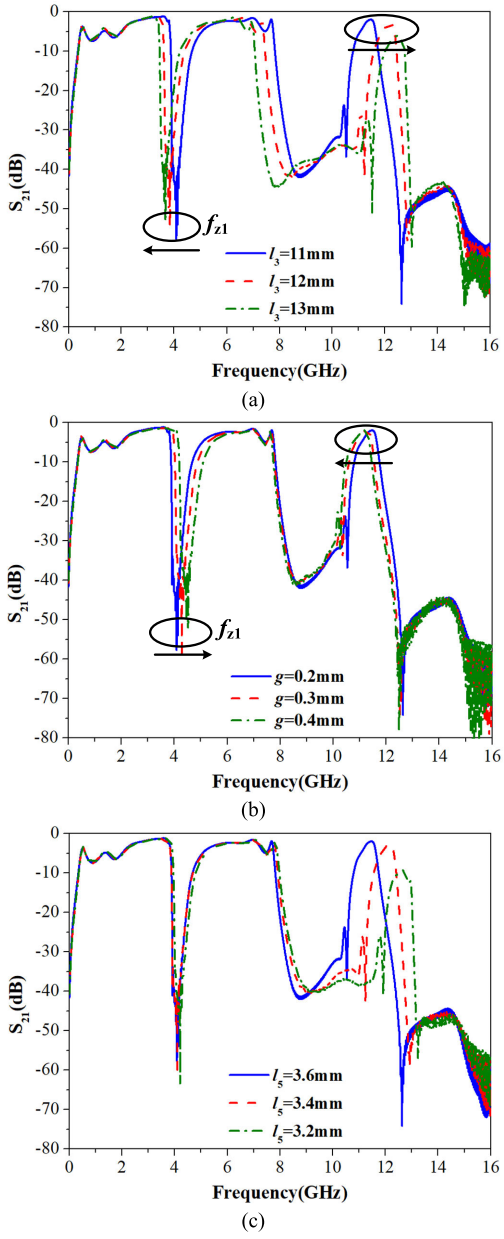

FIGURE 4. Variations of the transmission coefficients S_{21} with respect to geometrical parameters: (a) l_3. (b) g. (c) l_5.

It is worth noting that the variations of key parameters shown in Fig. 4 have no influence on the lower edge of the first passband, which demonstrates that the lowest cut off frequency of SSPPs is only determined by the conversion parts and the single conductor transmission line without corrugated strips, as shown in Fig. 6. The field conversion process from TEM mode of CPW to TM mode of single conductor is similar to that in [9]. It is found that the electromagnetic waves are mainly restricted between the single conductor transmission line and flaring grounds. Thus, a larger transverse distance between single conductor transmission line and flaring grounds should be needed to achieve good impedance match and smooth field conversion for lower passband. However, the transverse dimension of flaring grounds is always finite in

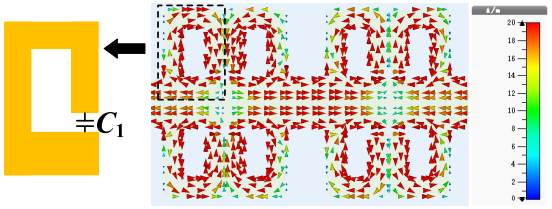

FIGURE 5. Current distribution of SSPPs unit cell at 11.4GHz.

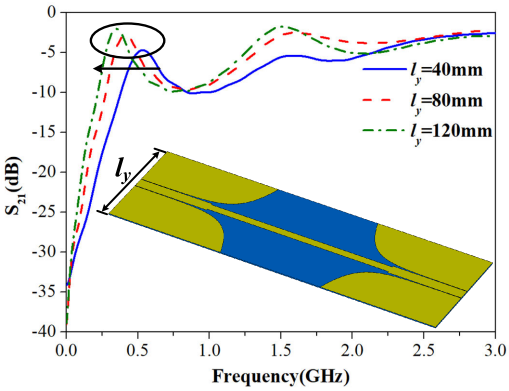

FIGURE 6. Influence of l_y on the lower edge of the first passband.

practical filter design, which will block the signal propagation and produce the lower edge of the first passband owing to the mismatching at lower frequencies. The influence of width l_y on the lower edge of first passband is illustrated in Fig. 6. It is clear that the lower edge of first passband shifts to lower frequencies by increasing l_y, which validates the theory given above.

B. EQUIVALENT TRANSMISSION LINE MODEL AND CIRCUIT ANALYSIS

By referring to the ground plane at infinity [27], [41], the equivalent transmission line models have been established to further explain operating principle of the proposed SSPPs-based filter. Fig. 7(a) and (b) are the equivalent circuit models for the conversion part and SSPPs unit cell, respectively. For the simplicity of analysis, Fig. 8(a) compares the transmission coefficients S_{21} obtained from full-wave simulation and transmission line model with only one SSPPs unit cell, and good agreement between them can be found. It is observed that there are two transmission zeros appearing at 4.05 GHz and 9.75 GHz respectively, which are generated by the resonance of SSPPs unit cell. In order to explain the principle of these two transmission zeros, analytic equations have been derived based on the equivalent circuit model of SSPPs unit cell. As shown in Fig. 7(b), the entire two-port network of SSPPs unit cell is formed by the parallel connection of transmission line model (Z_1, θ_1) and two same subnetworks. The subnetwork is formed by the cascade connection of transmission line models (Z_2, θ_2), (Z_o, Z_e, θ_3) and (Z_2, θ_2) in sequence. According to the transmission line theory, the ABCD matrix of the subnetwork can be derived as:

$$M_{sub} = \begin{bmatrix} A & B \\ C & D \end{bmatrix}_{sub} = M_2 \times M_c \times M_2 \qquad (2)$$

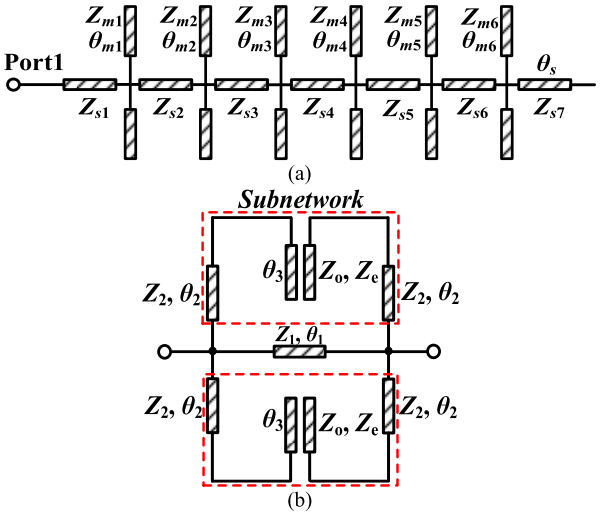

FIGURE 7. Analysis of equivalent transmission line model. The initial circuit parameters are extracted by the method given in [27], [41] and the final parameter values are obtained by curve-fitting. (a) Conversion part. (b) Proposed SSPPs unit cell.

where M_2 and M_c are the ABCD matrixes of the transmission line models (Z_2, θ_2) and coupled-stubs (Z_o, Z_e, θ_3) respectively, and are expressed as:

$$M_2 = \begin{bmatrix} \cos\theta_2 & jZ_2\sin\theta_2 \\ jY_2\sin\theta_2 & \cos\theta_2 \end{bmatrix} \tag{3a}$$

$$M_c = \begin{bmatrix} \dfrac{Z_e+Z_o}{Z_e-Z_o} & -j\dfrac{2Z_eZ_o\cot\theta_3}{Z_e-Z_o} \\ \dfrac{2j}{(Z_e-Z_o)\cot\theta_3} & \dfrac{Z_e+Z_o}{Z_e-Z_o} \end{bmatrix} \tag{3b}$$

Due to the parallel connection of two identical subnetworks and transmission line model (Z_1, θ_1), the total admittance matrix of the SSPPs unit cell Y_{total} can be derived as the matrix summation of two subnetworks and the transmission line model (Z_1, θ_1), as expressed as follows:

$$Y_{total} = Y_{sub} + Y_1 + Y_{sub} \tag{4}$$

where Y_{sub} and Y_1 are the admittance matrixes of subnetwork and transmission line model (Z_1, θ_1), respectively. Thus, the total transfer admittance of SSPPs unit cell $Y_{total,21}$ can be expressed as:

$$Y_{total,21} = 2Y_{sub,21} + Y_{1,21} \tag{5}$$

According to the microwave network theory, the conversion relation between ABCD and admittance matrixes is expressed as:

$$Y_{21} = -\frac{1}{B} \tag{6}$$

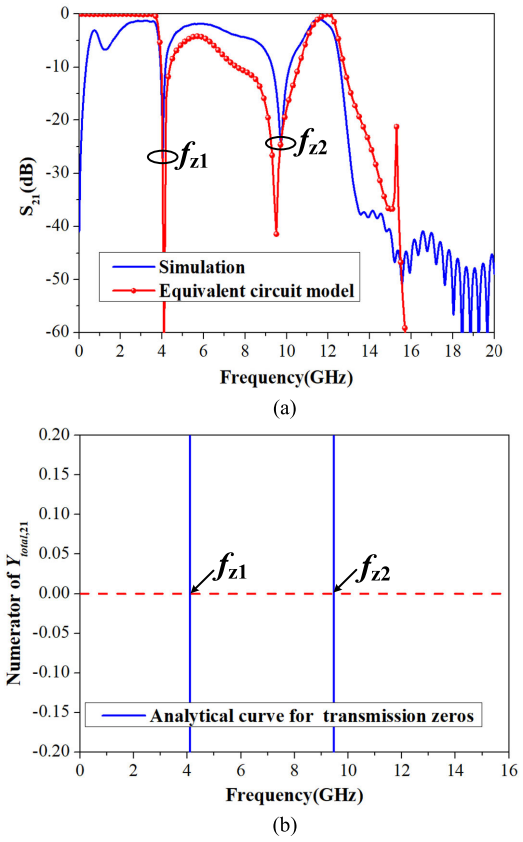

FIGURE 8. (a) Comparison of transmission coefficients S_{21} obtained from CST simulation and transmission line model with only one SSPPs unit cell. (b) Analytical curve for predicting transmission zeros.

Thus, the total transfer admittance $Y_{total,21}$ is derived (7), as shown at the bottom of this page:

It is known that the transmission zeros will appear when total transfer admittance equals to zero. Thus, the analytical equations for two transmission zeros can be derived as:

$$(Z_e - Z_o)\,Z_1\sin\theta_1 - Z_2^2\sin^2\theta_2\tan\theta_3 - Z_oZ_e\cos^2\theta\cot\theta_3 + (Z_e+Z_o)\,Z_2\sin\theta_2\cos\theta_2 = 0 \tag{8}$$

The analytical curve of equation (8) is presented in Fig. 8(b) to predict two transmission zeros. As can be seen, two transmission zeros, represented by the crossover points of analytical curve with $y = 0$, are located at 4.1GHz and 9.45 GHz, respectively. The good consistency with simulation results 4.05GHz and 9.75GHz has validated the effectiveness of the proposed equivalent circuit model and equation (8) for predicting filter performances. The small discrepancies between transmission zeros obtained from equation (8) and simulations are caused by the inaccuracy of circuit parameter extractions. In addition, the third passband is determined by the conversion part and proposed SSPPs transmission structure. The tedious formula derivation is not

$$Y_{total,21} = -j\frac{Z_e - Z_o}{Z_2\sin\theta_2\cos\theta_2\,(Z_e+Z_o) - Z_2^2\sin^2\theta_2\tan\theta_3 - Z_eZ_o\cos^2\theta_2\cot\theta_3} + j\frac{1}{Z_1\sin\theta_1} \tag{7}$$

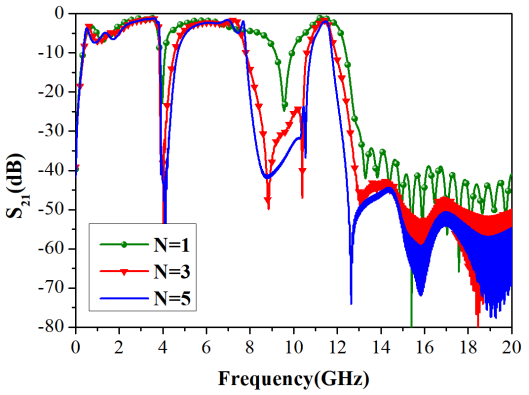

FIGURE 9. The simulated transmission coefficients S_{21} with different numbers of SSPPs unit cell N.

given here for conciseness. Fig. 9 investigates the influence of SSPPs unit cell numbers N on the filter performances. It can be seen that the first and second passbands are almost unchanged while the first stopband are gradually broadened due to the characteristic of periodic structures with the increase of N. Particularly, increasing number of SSPPs unit cell has significant influence on the second stopband. In the case of N=1, the number of SSPPs unit cell is too small to make the proposed filter be endowed with the cutoff frequency of SSPPs. In this scenario, the second stopband is generated by the resonance of SSPPs unit cell. However, with the increase of N, the second stopband will be determined by the SSPPs cutoff frequency, and the resonant frequency of SSPPs unit cell cannot be observed since it is higher than the SSPPs cutoff frequency. Thus, the second stopband is greatly broadened in the case of N=3 or 5. Meanwhile, increasing N has little influence on the transmission pole of the third passband, but narrowing the passband bandwidth. This phenomenon can be attributed to that the resonant tunneling effect is strengthened with the increase of the number of stages of periodic unit cells. In order to achieve the tri-band bandpass performances with excellent frequency selectivity, the number of SSPPs unit cell is finally chosen as 5 in this design.

III. EXPERIMENTAL RESULTS AND DISCUSSION

To validate the proposed filter performances, a prototype with 5 SSPPs unit cells has been fabricated by using printed circuit board technology, as shown in Fig. 10(a). As can be observed, two standard SMA connectors are assembled at the ends of CPWs, which are used to feed or receive guided wave energy. A vector network analyzer (Keysight PNA N5224A) is used for performance measurements. The measured transmission and reflection coefficients are depicted in Fig. 10(b) and (c) respectively to compare with the simulations, where good agreement can be observed. The measurement results have demonstrated that the proposed SSPPs-based filter can achieve good tri-band bandpass performance with superior frequency selectivity. However, the measured transmission pole of the third passband has little deviation compared with the simulation

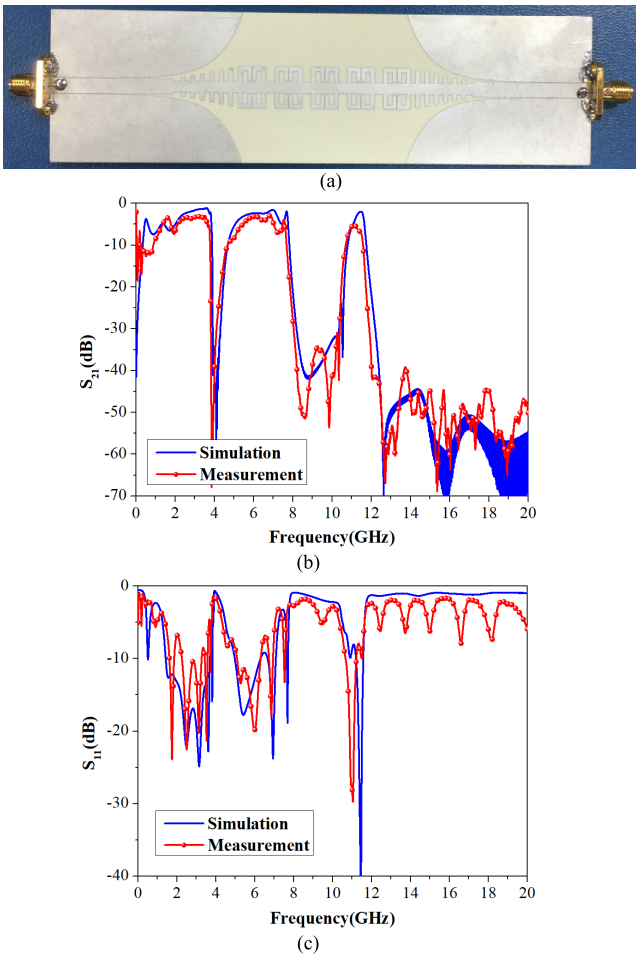

FIGURE 10. (a) Photograph of the fabricated SSPPs-based filter. (b) Comparison of transmission coefficient S_{21} between simulation and measurement. (c) Comparison of reflection coefficient S_{11} between simulation and measurement.

result, which is mainly caused by fabrication error. Moreover, the measured S_{21} at the transmission pole of the third passband is 3dB lower than the simulated one. The discrepancy is mainly attributed to the unstable dielectric loss in high frequencies and the extra conductor loss of SMA connectors used in measurements.

Table 1 compares the filter performances with related works in the state of the art. As can be observed, our work has proposed a novel tri-band bandpass filter based on the concept of multi-mode SSPPs, which indicates that the proposed SSPPs-based filter operates in different mechanism compared with other works. It is clear that the proposed SSPPs-based filter shows evident advantages including lower operating frequencies, relatively wide passband, and relatively small geometric length, owing to the superiority of multi-mode SSPPs unit cell. However, the insertion loss within three passbands is a little bit large compared with other works. This is because that the conductor is plated by tin, which leads to relatively higher conductor loss compared with copper used in other works.

Fig. 11(a) depicts the simulated loss ratios caused by different factors. It is clear that radiation loss is the main

TABLE 1. Performance comparison with related works.

Ref.	Responses	Central Frequencies (GHz)	Bandwidth (S_{11}<-10dB)	Insertion loss (dB)	Length (mm)	Type
[21]	Single passband	16.7	57.5%	0.5	125	Hybrid SIW/HMSIW and SSPPs
[22]	Single passband	21	43.8%	1.02	90	
[23]	Single passband	23.85	69.77	0.8	79.2	
[24]	Single passband	8.5	35.3%	1.5	263	Multi-stage SSPPs coupled to resonators
[27]	Single passband	8.5	35.2%	1.5	215	
[32]	Dual-passband	3.75, 9	146%, 11%	1.5, 2	>150	SSPPs loading extra resonators
[35]	Dual-passband	4.8, 5.7	5.2%, 8.2%	2.2, 2.17	43	SPPs-like induced by structural SIWs
[38]	Single-passband	4.4	53	1	>20	Multi-mode localized SPPs
This work	**Tri-passband**	**2.9, 5.6, 11**	**45.8%, 17.8%, 6.4%**	**3.0, 3.1, 5.2**	**144**	**Multi-mode SSPPs**

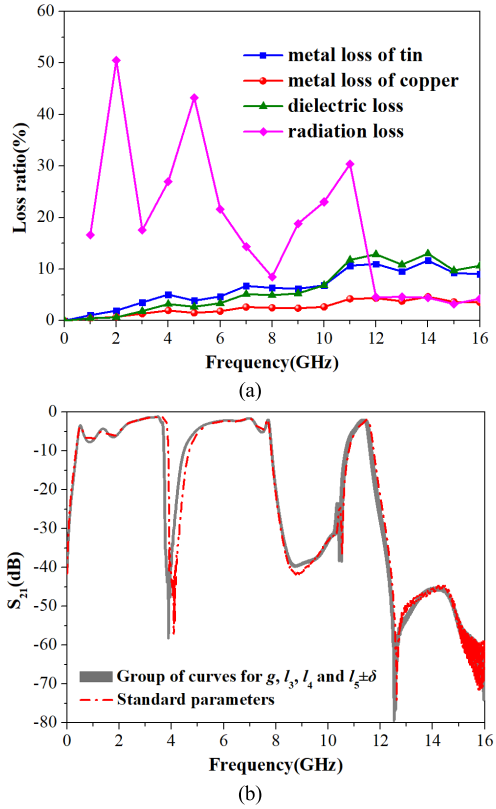

FIGURE 11. (a) Ratios of total loss. (b) Influence of fabrication error on the filter performance.

source contributing to the high transmission loss in the lower frequencies, which is mainly caused by the conversion parts [42]. In addition, larger metal loss is observed when conductor material is chosen as tin instead of copper especially for higher frequencies, validating the relatively higher transmission loss of measurements compared with other designs using copper. The standard printed circuit board technology is utilized to fabricate the proposed tri-band filter. The maximum fabrication tolerance in this process is $\delta = 0.5$mil, namely, 0.0127mm. Thus, the influence of key parameters with maximum fabrication error has been investigated in Fig. 11(b). As can be observed, the filter performance shows good stability with respect to fabrication error.

IV. CONCLUSION

In summary, a novel SSPPs-based filter is proposed in this paper to achieve tri-band bandpass performance based on the concept of multi-mode resonator. Due to the multiple resonance of SSPPs unit cell, the proposed filter can produce a stopband under the frequencies supporting SSPPs mode propagation, and support resonant tunneling effect above the SSPPs cutoff frequency. As a demonstration, a filter prototype has been fabricated and measured. The measurements show good consistency with the simulations. The superior tri-band bandpass performances of the proposed filter make it possible for promising applications in modern multi-band wireless systems.

REFERENCES

[1] W. L. Barnes, A. Dereux, and T. W. Ebbesen, "Surface plasmon subwavelength optics," *Nature*, vol. 424, no. 6950, pp. 824–830, Aug. 2003.
[2] S. A. Maier, *Plasmonics: Fundamentals and Applications*. New York, NY, USA: Springer, 2007.
[3] E. Ozbay, "Plasmonics: Merging photonics and electronics at nanoscale dimensions," *Science*, vol. 311, no. 5758, pp. 189–193, Jan. 2006.
[4] A. V. Zayats, I. I. Smolyaninov, and A. A. Maradudin, "Nano-optics of surface plasmon polaritons," *Phys. Rep.*, vol. 408, nos. 3–4, pp. 131–314, Mar. 2005.
[5] D. K. Gramotnev and S. I. Bozhevolnyi, "Plasmonics beyond the diffraction limit," *Nature Photon.*, vol. 4, no. 2, pp. 83–91, Feb. 2010.
[6] Q. Gan, F. J. Bartoli, and Z. H. Kafafi, "Plasmonic-enhanced organic photovoltaics: Breaking the 10% efficiency barrier," *Adv. Mater.*, vol. 25, no. 17, pp. 2385–2396, May 2013.
[7] J. B. Pendry, "Mimicking surface plasmons with structured surfaces," *Science*, vol. 305, no. 5685, pp. 847–848, Aug. 2004.

[8] F. J. Garcia-Vidal, L. Martín-Moreno, and J. B. Pendry, "Surfaces with holes in them: New plasmonic metamaterials," *J. Opt. A, Pure Appl. Opt.*, vol. 7, no. 2, pp. S97–S101, Feb. 2005.

[9] H. F. Ma, X. Shen, Q. Cheng, W. X. Jiang, and T. J. Cui, "Broadband and high-efficiency conversion from guided waves to spoof surface plasmon polaritons," *Laser Photon. Rev.*, vol. 8, no. 1, pp. 146–151, Jan. 2014.

[10] J. Wu, D. Hou, T. Yang, I. Hsieh, Y. Kao, and H. Lin, "Bandpass filter based on low frequency spoof surface plasmon polaritons," *Electron. Lett.*, vol. 48, no. 5, p. 269, 2012.

[11] S. Shen, B. Xue, M. Yu, and J. Xu, "A novel three-dimensional integrated spoof surface plasmon polaritons transmission line," *IEEE Access*, vol. 7, pp. 26900–26908, 2019.

[12] Z. Yang, B. Zhang, W. Chen, and T. Yang, "Rejection of spoof SPPs using the second resonant mode of vertical split-ring resonator," *IEEE Microw. Wireless Compon. Lett.*, vol. 29, no. 1, pp. 23–25, Jan. 2019.

[13] Y. J. Guo, K. D. Xu, Y. Liu, and X. Tang, "Novel surface plasmon polariton waveguides with enhanced field confinement for microwave-frequency ultra-wideband bandpass filters," *IEEE Access*, vol. 6, pp. 10249–10256, 2018.

[14] J. Wang, L. Zhao, and Z.-C. Hao, "A band-pass filter based on the spoof surface plasmon polaritons and CPW-based coupling structure," *IEEE Access*, vol. 7, pp. 35089–35096, 2019.

[15] S.-Y. Zhou, S.-W. Wong, J.-Y. Lin, L. Zhu, Y. He, and Z.-H. Tu, "Four-way spoof surface plasmon polaritons splitter/combiner," *IEEE Microw. Wireless Compon. Lett.*, vol. 29, no. 2, pp. 98–100, Feb. 2019.

[16] M. Aghadjani, M. Erementchouk, and P. Mazumder, "Spoof surface plasmon polariton beam splitter," *IEEE Trans. THz Sci. Technol.*, vol. 6, no. 6, pp. 832–839, Nov. 2016.

[17] A. Kandwal, Q. Zhang, X.-L. Tang, L. W. Liu, and G. Zhang, "Low-profile spoof surface plasmon polaritons traveling-wave antenna for near-endfire radiation," *IEEE Antennas Wireless Propag. Lett.*, vol. 17, no. 2, pp. 184–187, Feb. 2018.

[18] Q.-L. Zhang, B.-J. Chen, Q. Zhu, K. F. Chan, and C. H. Chan, "Wideband millimeter-wave antenna with low cross polarization based on spoof surface plasmon polaritons," *IEEE Antennas Wireless Propag. Lett.*, vol. 18, no. 8, pp. 1681–1685, Aug. 2019.

[19] K. Zhuang, J. Geng, K. Wang, H. Zhou, Y. Liang, X. Liang, W. Zhu, R. Jin, and W. Ma, "Pattern reconfigurable antenna applying spoof surface plasmon polaritons for wide angle beam steering," *IEEE Access*, vol. 7, pp. 15444–15451, 2019.

[20] X. Du, H. Li, and Y. Yin, "Wideband fish-bone antenna utilizing odd-mode spoof surface plasmon polaritons for end-fire radiation," *IEEE Trans. Antennas Propag.*, to be published.

[21] Q. Zhang, H. C. Zhang, H. Wu, and T. J. Cui, "A hybrid circuit for spoof surface plasmons and spatial waveguide modes to reach controllable band-pass filters," *Sci. Rep.*, vol. 5, Nov. 2015, Art. no. 16531.

[22] D.-F. Guan, P. You, Q. Zhang, K. Xiao, and S.-W. Yong, "Hybrid spoof surface plasmon polariton and substrate integrated waveguide transmission line and its application in filter," *IEEE Trans. Microw. Theory Techn.*, vol. 65, no. 12, pp. 4925–4932, Dec. 2017.

[23] L. Zhao, Y. Li, Z.-M. Chen, X.-H. Liang, J. Wang, X. Shen, and Q. Zhang, "A band-pass filter based on half-mode substrate integrated waveguide and spoof surface plasmon polaritons," *Sci. Rep.*, vol. 9, Nov. 2015, Art. no. 13429.

[24] J. Y. Yin, J. Ren, H. C. Zhang, B. C. Pan, and T. J. Cui, "Broadband frequency-selective spoof surface plasmon polaritons on ultrathin metallic structure," *Sci. Rep.*, vol. 5, no. 8165, pp. 1–5, Feb. 2015.

[25] R. K. Jaiswal, N. Pandit, and N. P. Pathak, "Spoof surface plasmon polaritons based reconfigurable band-pass filter," *IEEE Photon. Technol. Lett.*, vol. 31, no. 3, pp. 218–221, Feb. 1, 2019.

[26] R. K. Jaiswal, N. Pandit, and N. P. Pathak, "Spoof plasmonic-based band-pass filter with high selectivity and wide rejection bandwidth," *IEEE Photon. Technol. Lett.*, vol. 31, no. 15, pp. 1293–1296, Aug. 1, 2019.

[27] L. Zhao, X. Zhang, J. Wang, W. Yu, J. Li, H. Su, and X. Shen, "A novel broadband band-pass filter based on spoof surface plasmon polaritons," *Sci. Rep.*, vol. 6, Oct. 2016, Art. no. 36069.

[28] S. Zhao, H. C. Zhang, J. Zhao, and W. X. Tang, "An ultra-compact rejection filter based on spoof surface plasmon polaritons," *Sci. Rep.*, vol. 7, Sep. 2017, Art. no. 10576.

[29] Q. Zhang, H. C. Zhang, J. Y. Yin, B. C. Pan, and T. J. Cui, "A series of compact rejection filters based on the interaction between spoof SPPs and CSRRs," *Sci. Rep.*, vol. 6, no. 28256, pp. 1–10, Jun. 2016.

[30] A. K. Horestani, W. Withayachumnankul, A. Chahadih, A. Ghaddar, M. Zehar, D. Abbott, C. Fumeaux, and T. Akalin, "Metamaterial-inspired bandpass filters for Terahertz surface waves on Goubau lines," *IEEE Trans. THz Sci. Technol.*, vol. 3, no. 6, pp. 851–858, Nov. 2013.

[31] E. Elrifai, M. Grzeskowiak, G. Lissorgues, F. Deshours, C. Bourcier, G. Carrer, E. Richalot, and O. Picon, "60 GHz square open-loop resonator (SOLR) based on planar Goubau line (PGL) technology," *IET Microw., Antennas Propag.*, vol. 13, no. 5, pp. 660–665, Apr. 2019.

[32] B. C. Pan, Z. Liao, J. Zhao, and T. J. Cui, "Controlling rejections of spoof surface plasmon polaritons using metamaterial particles," *Opt. Express*, vol. 22, no. 11, p. 13940, Jun. 2014.

[33] S. Liao, C. Qi, and Q. Xue, "Effective bandpass filtering for spoof surface plasmon polariton transmission lines," *Appl. Phys. Express*, vol. 12, no. 5, May 2019, Art. no. 054501.

[34] Z. Xu, S. Liu, S. Li, H. Zhao, L. Liu, and X. Yin, "Tunneling of spoof surface plasmon polaritons through magnetoinductive metamaterial channels," *Appl. Phys. Express*, vol. 11, no. 4, Apr. 2018, Art. no. 042002.

[35] N. Cselyuszka, Z. Sakotic, G. Kitic, V. Crnojevic-Bengin, and N. Jankovic, "Novel dual-band band-pass filters based on surface plasmon polariton-like propagation induced by structural dispersion of substrate integrated waveguide," *Sci. Rep.*, vol. 8, May 2018, Art. no. 8332.

[36] L. Zhu, S. Sun, and W. Menzel, "Ultra-wideband (UWB) bandpass filters using multiple-mode resonator," *IEEE Microw. Wireless Compon. Lett.*, vol. 15, no. 11, pp. 796–798, Nov. 2005.

[37] X. Liu, Y. Feng, B. Zhu, J. Zhao, and T. Jiang, "High-order modes of spoof surface plasmonic wave transmission on thin metal film structure," *Opt. Express*, vol. 21, no. 25, Dec. 2013, Art. no. 31155.

[38] X. Zhang, D. Bao, J. F. Liu, and T. J. Cui, "Wide-bandpass filtering due to multipole resonances of spoof localized surface plasmons," *Annalen Der Physik*, vol. 530, no. 11, Nov. 2018, Art. no. 1800207.

[39] Z. X. Wang, H. C. Zhang, J. Lu, P. Xu, L. W. Wu, R. Y. Wu, and T. J. Cui, "Compact filters with adjustable multi-band rejections based on spoof surface plasmon polaritons," *J. Phys. D, Appl. Phys.*, vol. 52, no. 2, Jan. 2019, Art. no. 025107.

[40] G. Goubau, "Single-conductor surface-wave transmission lines," *Proc. IRE*, vol. 39, no. 6, pp. 619–624, Jun. 1951.

[41] A. Kianinejad, Z. N. Chen, and C.-W. Qiu, "Design and modeling of spoof surface plasmon modes-based microwave slow-wave transmission line," *IEEE Trans. Microw. Theory Techn.*, vol. 63, no. 6, pp. 1817–1825, Jun. 2015.

[42] Z. Xu, S. Li, X. Yin, H. Zhao, and L. Liu, "Radiation loss of planar surface plasmon polaritons transmission lines at microwave frequencies," *Sci. Rep.*, vol. 7, Jul. 2017, Art. no. 6098.

HONGXIN ZHAO (Member, IEEE) received the B.S. degree in radio communication techniques, and the M.S. and Ph.D. degrees in microwave techniques from Southeast University (SEU), Nanjing, China, in 1993, 1996, and 2003, respectively. He is currently an Associate Professor with the School of Information Science and Engineering, SEU. He has been involved in research and developments of RF front ends for mobile communication, FMCW, RFID, and wireless channel measurement systems. His current research interests include microwave devices, circuits, millimeter-wave wireless communication systems, and embedded digital signal processing techniques.

PENG ZHOU (Student Member, IEEE) received the B.S. and M.S. degrees from Nanjing Normal University, Nanjing, China, in 2016 and 2019, respectively. He is currently pursuing the Ph.D. degree in electromagnetic field and microwave technique with Southeast University, Nanjing. His current research interests include the analysis of signal integrity in high-speed digital circuits and systems, and microwave circuit design.

ZHIXIA XU (Student Member, IEEE) was born in Wuxi, China. He received the B.Eng. degree in electronic information science and technology from Dalian Maritime University, Dalian, China, in 2015, and the Ph.D. degree in electromagnetic field and microwave technique from Southeast University, Nanjing, China, in 2019. From 2018 to 2019, he worked as a Visiting Graduate Student with the University of California, San Diego, CA, USA. His current research interests include antenna theory and designs, periodic structures, surface waves, and photonic topological insulators.

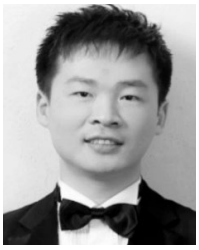

SHUNLI LI (Member, IEEE) was born in Liaocheng, Shandong, China, in 1984. He received the B.S. degree in science and technology of electronic information and the M.S. degree in radio physics from Shandong University, in 2007 and 2010, respectively, and the Ph.D. degree in electromagnetic field and microwave technology from the State Key Laboratory of Millimeter Waves, Southeast University (SEU), in 2015. In 2015, he joined the Department of Electrical and Computer Engineering, National University of Singapore, as a Research Fellow. In 2017, he joined the State Key Laboratory of Millimeter Waves, SEU, with interests in ultrawideband antennas and arrays, time-domain analysis, microwave passive devices, and short-pulse antennas and networks.

MEI YANG (Member, IEEE) was born in Shandong, China, in 1985. She received the B.S. degree in electronic information engineering and the M.S. degree in electromagnetic field and microwave technology from Shandong University (SDU), in 2007 and 2010, respectively, and the Ph.D. degree in electromagnetic field and microwave technology from Southeast University (SEU), in 2015. She has been with the College of Telecommunications and Information Engineering, Nanjing University of Posts and Telecommunications, since 2015. Her research interests include ultrawideband antennas and arrays, pulse antennas and lens antennas, and wireless communication systems.

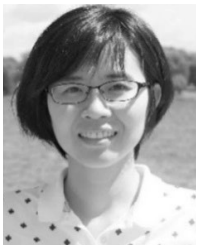

LEILEI LIU (Member, IEEE) received the B.Sc. and Ph.D. degrees in electromagnetic and microwave technology from Southeast University, Nanjing, China, in 2003 and 2009, respectively. She studied in Linnaeus University, Kalmar, Sweden, as an International Student, in 2004. From 2015 to 2016, she was a Visiting Scholar with the Poly-Grames Research Center, Montreal, QC, Canada. Since 2009, she has been an Associate Professor with the Nanjing University of Posts and Telecommunications, Nanjing. Her current research interests include slot antennas, leaky-wave antennas, and metamaterials.

XIAOXING YIN (Member, IEEE) was born in Taiyuan, China. He received the B.Sc. degree in radio engineering, and the M.Sc. and Ph.D. degrees in electrical engineering from the Nanjing Institute of Technology (now Southeast University), Nanjing, China, in 1983, 1989, and 2001, respectively. From 1983 to 1986 and 1989 to 1998, he was with the Department of Physics, University of Petroleum, Dongying, China, where he was involved in logging methods and instruments. Since 2001, he has been a Lecturer with the State key Laboratory of Millimeter Waves, Southeast University, where he is currently a Professor. He has authored or coauthored 63 technical papers. He holds over 30 patents. His current research interests include computational electromagnetics, microwave components and systems, and antennas.